JOURNAL of
MATERIALS and MECHATRONICS:A

e-ISSN 2717-8811
JournalMM, 2021, 2(1), 37-50

Araştırma Makalesi / Research Article

Digital Compass Calibration Using Particle Swarm Optimization and Least Squares Method

Türkay PEKTÜRK[1], Sıtkı KOCAOĞLU[2]*

[1] Kırklareli Üniversitesi, Mühendislik Fakültesi, Elektrik Elektronik Mühendisliği Bölümü, Kırklareli, Türkiye,
ORCID ID: https://orcid.org/0000-0002-6610-5425, turkaypekturk@gmail.com
[2] Kırklareli Üniversitesi, Teknik Bilimler Meslek Yüksekokulu, Elektronik ve Otomasyon Bölümü, Kırklareli, Türkiye,
ORCID ID: https://orcid.org/0000-0003-1048-9623, sitki.kocaoglu@klu.edu.tr

Geliş/ Recieved: 10.12.2020; **Kabul / Accepted:** 22.02.2021

ABSTRACT: Recently, electronic compass sensors have become very common, due to their small size and low price. Sensor output information turns out to be incorrect if the magnetometers and accelerometers in the structure of these sensors are not calibrated. The main reason for such an error could be the slope value that is generated because of not placing the sensor parallel to the ground. Moreover, zero value inequalities between the axes of multi-axis sensors, offset errors, and scaling errors cause drift in the compass sensor output. In order to fix the problems, the study uses the methods of Particle Swarm Optimization Algorithm and Least Squares for the calibration of magnetometer and accelerometer. The results indicate that the calibration process can be successfully performed using these methods.

Keywords: Compass, Calibration, Particle Swarm Optimization, Least Squares, IMU.

*Sorumlu yazar / Corresponding author: sitki.kocaoglu@klu.edu.tr

Bu makaleye atıf yapmak için /To cite this article

Pektürk, T., Kocaoğlu, S. (2021). Digital Compass Calibration Using Particle Swarm Optimization and Least Squares Method. Journal of Materials and Mechatronics: A (JournalMM), 2(1), 37-50.

Parçacık Sürü Optimizasyonu ve En Küçük Kareler Yöntemi Kullanılarak Dijital Pusula Kalibrasyonu

ÖZET: Elektronik pusula sensörleri, küçük boyutları ve düşük fiyatları sayesinde son yıllarda oldukça yaygın hale gelmiştir. Bu sensörlerin yapısında bulunan manyetometreler ve ivmeölçerlerin kalibre edilmediği durumlarda sensör çıkış bilgisi hatalı olmaktadır. Bunun temel sebebi sensörün kullanım alanında zemin yüzeyine paralel tutulamaması ve bir eğim değerine sahip olmasıdır. Ayrıca çok eksenli sensörlerin eksenleri arasındaki sıfır değer eşitsizlikleri, ofset hataları ve ölçekleme hataları da pusula sensör çıkışında kaymaya neden olur. Bu çalışmada, bahsedilen problemlerin giderilmesi için, manyetometre ve ivmeölçer kalibrasyonu Parçacık Sürüsü Optimizasyon Algoritması ve En Küçük Kareler Yöntemi kullanılarak yapılmıştır. Çalışmada önerilen yöntemle elde edilen sonuçlar, kalibrasyon işleminin bu yöntem kullanılarak başarıyla yapılabileceğini göstermiştir.

Anahtar Kelimeler: Pusula, Kalibrasyon, Parçacık Sürü Optimizasyonu, En Küçük Kareler, IMU.

1. INTRODUCTION

With the emergence of microelectromechanical systems (MEMS) technology, the dimensions of the mechanical sensors are reduced to a measure that can be expressed in millimeters and their energy consumption is reduced to very low levels (Li et al., 2009). This situation has led to the emergence of many new application areas and MEMS technology has spread rapidly and become quite economical. This technology, which has also entered into mobile phones today, is widely used in many applications such as navigation, robotics, unmanned vehicles, medical devices, automotive, computer technologies, wearable devices, virtual reality, and military defense systems (Petrucha and Kaspar, 2009).

In addition to these advantages of MEMS sensors, there are some engineering challenges; especially surface micro-processing and extremely low-cost variations need to be mentioned. Since the accuracy and sensitivity performances of the sensors which are produced by surface micro-processing are low, it is necessary to minimize the errors by using mathematical and heuristic methods in applications.

Magnetic compasses have been used for navigation for centuries. Today, advances in technology have led to the emergence of solid-state electronic compasses based on magnetic sensors and acceleration-based slope sensors. Electronic compasses have many advantages over traditional needle type or Gimbaled compasses in terms of shock and vibration resistance, electronic compensation for stray field effects, and direct interface to electronic navigation systems. Usually compasses are hand-held, attached to an airplane, or housed on a vehicle over rough terrain. This makes it difficult to determine the azimuth or its direction as the compass is not always horizontal to the earth's surface. The error caused by tilt angles can be quite substantial. A typical method of correcting the compass slope is to use a tilt sensor to determine the turn and tilt angles (Xisheng et al., 2009; Kuşçu, et al., 2018).

Three-dimensional magnetic digital compasses are widely used as handheld navigation devices. Anisotropic magneto resistivity (AMR) sensors and MEMS accelerometers in compasses are used to obtain geomagnetic field and gravitational field (Barbert and Arrott, 1988; Caruso, 2000; Choudhury et al., 2008; P. Zhang et al., 2005). Attitude and heading can be calculated from two vectors using the following equations (Cho and Park, 2003):

$$\psi = tan^{-1}\left(\frac{-B_y\, cos\phi + B_z\, sin\phi}{B_x\, cos\theta + B_y\, sin\theta\, sin\phi + B_z\, sin\theta\, cos\phi}\right) \quad (1)$$

$$\theta = sin^{-1}\left(\frac{A_x}{A_z}\right) \quad (2)$$

$$\phi = sin^{-1}\left(\frac{A_y}{A_z}\right) \quad (3)$$

where θ and φ represent the sensor's angle calculated from the accelerometer readings and the roll, respectively. Ψ represents heading angle calculated from two sensor whose tilts are compensated. A_i and B_i (i = x, y, z), show the sensor readings of the three axes.

In (Fang et al., 2011), ellipsoid fitting (EF) is proposed to calibrate magnetometers without an external reference. In (Gietzelt et al. 2013), satisfactory results are received with accelerometers calibrated using EF. In (Vcelak et al., 2006), problems associated with EF used to prove the false attitudes. Later, many methods are proposed to compensate for these problems. In (Z. Zhang, 2015), an iterative algorithm is validated to ensure efficient calibration of magnetometers and accelerometers, but requires an external attitude reference. In (X. Li and Z. Li, 2012), it is assumed that the accelerometers provide an internal, pre-calibrated reference. The Deep Packet Inspection (DPI) algorithm is proposed to calibrate magnetometers. The experimental results are satisfactory, but in most cases, it is necessary to calibrate two area sensors.

PSO is an optimization algorithm inspired by the observation that the actions of some animals moving in a herd, while meeting their basic needs such as finding food, affect other individuals in the herd and reach the purpose of the herd more easily. Particle swarm optimization (PSO) is a parallel search technique developed by Kenney and Eberhart in 1995 (Bo and Hongxia, 2020). PSO is a stochastic optimization algorithm based on Swarm Intelligence Algorithm (SIA). It does not require much prior knowledge about initial parameter values, but provides a wide range of searches (Zhao et al., 2009). Each individual searching for the solution in PSO is called a particle, while the population containing the particles is called a herd. The fitness function is used to understand how close an individual is to the solution. This function could be a function that evaluates the suitability of the solution, taking into account the total value of the selected loads, taking our freighter example. The main purpose of this function is to measure how close we are to the real solution. While a particle is looking for the solution, its best state at that moment is called pbest, while the particle closest to the solution throughout the entire flock is called gbest.

In recent years, some researchers have used PSO to define control parameters (Bo and Hongxia, 2020; Zhao et al., 2009). Unfortunately, when the target function reaches the local optimal solution zone, convergence rates will likely slow down and fall to local optimal solutions in this method. Path planning is an important study area where PSO is used. In (Gong et al., 2013), an improved PSO is used to solve the shortest and safest path for a robot. Similarly, in (Mac et al., 2017), the shortest and smoothest path planning applied by using an improved PSO algorithm. In 2019, Wu used PSO algorithm to do coordinated path planning for unmanned aerial-aquatic vehicle. In (Das et al., 2016), an improved PSO and gravitational search algorithm is presented for path planning.

In this study, a tilt compensated digital compass application is carried out using a very low-cost MEMS sensor combining a three-axis magnetic field sensor and a three-axis acceleration sensor in a single case. The main purpose of this application is improving the measuring accuracy of IMU sensors. The errors and their reasons are mentioned and precautions to decrease the errors are taken.

In practice, sensor errors are examined, "Particle Swarm Optimization" and "Least squares" methods are used to eliminate the errors.

2. MATERIALS AND METHODS

In this study, GY-89 IMU module is used. Inside the module are LSM303D, L3GD20 and BMP180 units. LSM303D contains one 3-axis magnetometer and one 3-axis accelerometer. L3GD20 is a 3-axis gyroscope module. BMP180 is the absolute pressure sensor. Software configuration of the IMU module and sensor data reading are performed by the STM32 Smart microcontroller module over the I2C interface. The sensor data collected by the microcontroller has been exported over the NRF24L01 + RF communication module.

2.2 Magnetometer Calibration

In Figure 1, the dual axis comparative analysis of the uncalibrated magnetic field sensor used in the study is shown. The fact that XY (ZN), XZ (YN) and YZ (XN) charts are elliptical is related to the axes having different scaling values. This can be called a scaling error. Sensors with scaling errors produce different values when exposed to magnetic field in the same direction and equal intensity with their core axes. In addition, it is seen that the center points of the ellipses are also shifted from the origin. The reason for this is that the axes do not give zero (0) value at their outputs corresponding to the zero (0) gauss magnetic field value. This error is called an offset error. In the figure, the YZ (ZN) graph shows the change of the Z axis value (vertical) and the Y axis value (horizontal) when the sensor is rotated around the Z axis. Normally, the magnetic field value measured by the Y axis changes continuously during rotation, while the magnetic field measured by the Z axis does not change. For this reason, the graph is expected to be in the form of a straight line parallel to the horizontal axis. However, as can be seen in the figure, the magnetic field changes on the Y axis also affect the Z axis measurement. This indicates that the Y axis and the Z axis are not perpendicular to each other. A similar situation is also valid for XZ (ZN), XY (YN) charts. This error is called a cross-axis interaction error.

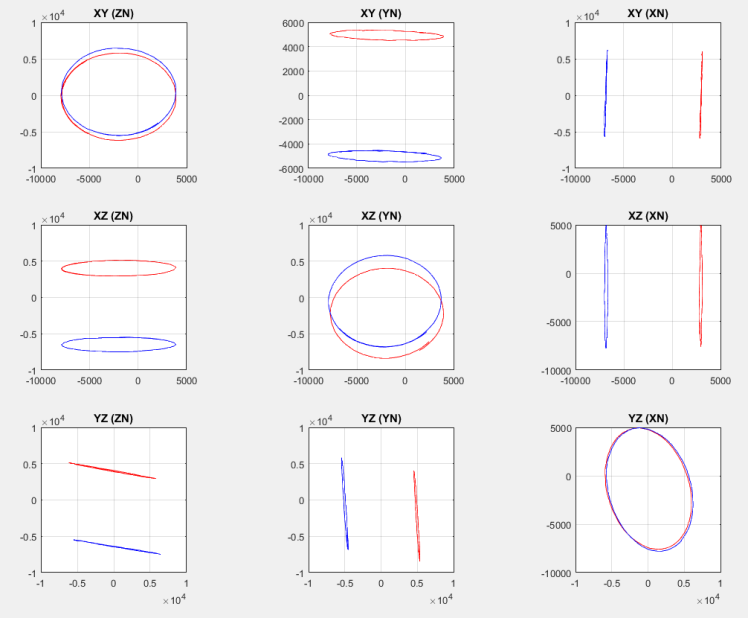

Figure 1. Magnetic field measurement results before calibration

Equation 4 shows the relationship between the actual magnetic field that the sensor is exposed to and the sensor output values. Here $[M]_{1x3}$ shows the real magnetic field value to which the sensor is exposed, and $[M_s]_{3x1}$shows the unwrought sample value taken from the sensor. $[M_c]_{3x3}$, $[M_s]_{3x3}$ and $[M_o]_{3x1}$ are the cross- axis effect correction matrix, scale factor correction matrix and offset error correction matrix, respectively. As a result of the calibration process, these three matrices will be obtained, which are used to correct errors in sensor measurements.

$$[M]_{1x3} = [M_c]_{3x3}[M_s]_{3x3}([M_m]_{3x1} - [M_o]_{3x1}) \quad (4)$$

The first thing to do in the calibration process is to roughly eliminate offset errors. Thus, the centers of the elliptical shapes formed by the measurements in the horizontal axes will be brought closer to the origin. For this, the offset values are calculated as follows by taking the average of the output values given by the axes in the vertical and upward positions (rotated 180 °) while the axes are perpendicular to the ground plane (Equations 5-7). Here X_o, Y_o and Z_o are the offset values for the X, Y and Z axes, respectively, XU_X, YU_Y and ZU_Z are the x values obtained with the X axis pointing upwards, the y values obtained with the Y axis pointing upward, and the z values obtained with the Z axis pointing upwards respectively and XD_X, YD_Y ve ZD_Z are x values obtained with the X axis pointing down, y values obtained with the Y axis pointing down, and z values obtained with the Z axis pointing down, respectively.

$$X_o = \frac{1}{2n}\left(\sum_{i=0}^{n} XU_{Xi} + \sum_{i=0}^{n} XD_{Xi}\right) \quad (5)$$

$$Y_o = \frac{1}{2n}\left(\sum_{i=0}^{n} YU_{Yi} + \sum_{i=0}^{n} YD_{Yi}\right) \quad (6)$$

$$Z_o = \frac{1}{2n}\left(\sum_{i=0}^{n} ZU_{Zi} + \sum_{i=0}^{n} ZD_{Zi}\right) \quad (7)$$

The offset values determined by calculating the offset values of each of the X, Y and Z axes are removed from all measurement results, thus offset errors are roughly eliminated.

In the next step, using the PSO, which is a heuristic optimization method, the interaction matrix between axes and offset correction values are found to make the already roughly calculated offset values more precise.

In the PSO method, there are pieces of data called randomly located particles in the possible solution space of the system. Each of these particles has speed and direction information that is changed randomly from iteration to iteration. In each iteration, the probable solution value contained by the particles is evaluated using a performance function. As a result of the evaluation, the value of the particle with the highest performance affects the speed and direction values of other particles in the next iteration. Thus, particles occupy a position in the solution space at a point in their tendency to approach the best available solution. The real or best solution is likely to be somewhere in the solution space, close to the best available solution. The effect of the best available solution value obtained in each iteration causes the particles to get closer and closer to each other in the solution space, and as the real solution approaches, all particles begin to cluster around a solution. This cycle continues until the result of the performance function reaches the desired value or stabilizes at a

certain value, and the data of the particle that provides the best value in the performance function becomes the solution value of the problem. Corrected results are obtained by multiplying the matrix created with the values found using the particle swarm algorithm with the sensor data vector (Equation 8). The matrix is formed as follows: X, Y and Z are the axis interference error and offset error corrected samples, Mx, My and Mz are the offset error roughly corrected samples and $P_{1\ldots9}$ are the parameters to be found with PSO (Kocabıçak and Demir, 2020; Kocaoğlu and Akdoğan, 2019).

$$[X\ Y\ Z] = [Mx\ My\ Mz\ 1]\begin{bmatrix} 1 & P_4 & P_7 \\ P_1 & 1 & P_8 \\ P_2 & P_5 & P_1 \\ P_3 & P_6 & P_9 \end{bmatrix} \tag{8}$$

Here, P3, P6 and P9 are the offset correction values of the X, Y and Z axes respectively, P1 and P2 are the interaction coefficients of the Y and Z sensor values on the X axis, P4 and P5 are respectively the action coefficients of the X and Z sensor values on the Y axis, P7 and P8 are respectively X and Y are the coefficients of the sensor values on the Z axis.

In the performance test function, 3 metrics are determined as success criteria. These are;

i) **The slope of the horizontal axis graph relative to the vertical axis:** The best case is that it is as close to zero as possible. To quantify this, the slopes of a total of 12 graphs obtained from the samples are calculated, the square root of the squares of these slopes are calculated and multiplied by a gain factor of 10000. The gain factor increases the effectiveness of the slope information, which normally takes values between 0 and 1, on the performance evaluation of the algorithm.

ii) **Shapes of horizontal axis charts: S**hapes should be like a circle. For this, the center point and the mean radius of the graph are determined. The perfect circle function is created accordingly. The corresponding angle for each data pair from the samples is found and the X and Y values corresponding to the same angle in the perfect circle function are calculated. The square root of the difference between the real sample and desired is calculated and the similarity value is determined. Similarity criterion is obtained by summing the similarity values for 6 graphs obtained from the samples.

iii) **Variance of the vector sum of X, Y and Z measurement values:** Calculation results for all sample points must be found on a sphere. In order to achieve this, it is necessary that the vector sum of X, Y and Z should give the radius of the sphere, so this value should not vary from sample to sample. With this aim in mind, the criterion value was determined by taking the calculated variance for all samples as $R = \sqrt{X^2 + Y^2 + Z^2}$.

Finally, the three criterion values are divided by the expected best values, added together and the performance value is obtained.

In the last step of the calibration, the least squares method is applied to the calibrated sensor data and scaling values are obtained in a way that fits the sensor values on the unit circle. Magnetic field measurement results after calibration are shown in Figure 2.

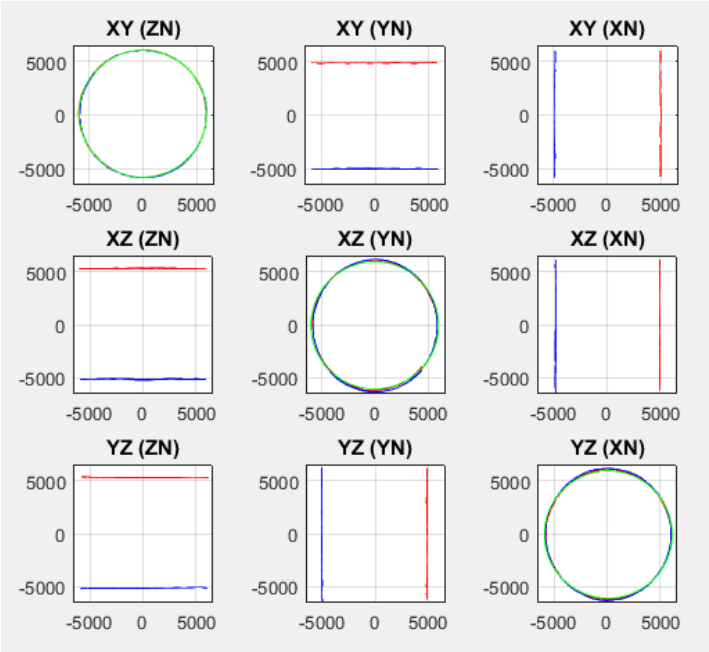

Figure 2. Magnetic field measurement results after calibration

2.2 Accelerometer Calibration

In accelerometer calibration, there are two calibration values for each axis of the sensor. These are the offset value that allows the sensor to produce a value of 0 when not subjected to any acceleration, and the scaling value that allows each of the three sensors to produce the same value when subjected to the same magnitude of acceleration. In the examples used for calibration, the sensor is calibrated for gravity acceleration (1g) as it is subjected only to gravitational acceleration. In Equation 9, A_a represents the calibrated sensor measurement values, A_m represents the raw sensor measurements, and A_c represents the calibration parameters.

$$[A_a] = [A_m][A_c] \tag{9}$$

When matrices are expressed explicitly;

$$[X, Y, Z] = \begin{bmatrix} A_x & A_y & A_z & 1 \end{bmatrix} \begin{bmatrix} P_1 & P_2 & P_3 \\ P_4 & P_5 & P_6 \\ P_7 & P_8 & P_9 \\ P_{10} & P_{11} & P_{12} \end{bmatrix} \tag{10}$$

Equation 10 contains the offset values of each axis in the last row of the calibration parameters matrix.

In the calibration process, the value sets, collected in 6 fixed positions such as XD, XU, YD, YU, ZD, ZU, are used. X, Y and Z are the sensor axes, U suffix refers to the upward direction according to gravity and the suffix D to the downward direction. Since the gravity value is taken as 1g after calibration, the value of the upward facing sensor according to gravity takes -1, and the value of the downward facing sensor takes 1. Horizontal axes will not be subject to any acceleration since they are perpendicular to gravity and will take zero value. Value sets are calculated through the following equations to represent the number of samples collected at the respective location.

$$\begin{aligned}
&\text{XD:} \quad [1 \quad 0 \quad 0]_{nx3} = [A_x\ A_y\ A_z\ 1]_{nx4}[A_c]_{4x3} \\
&\text{XU:} \quad [-1 \quad 0 \quad 0]_{nx3} = [A_x\ A_y\ A_z\ 1]_{nx4}[A_c]_{4x3} \\
&\text{YD:} \quad [0 \quad 1 \quad 0]_{nx3} = [A_x\ A_y\ A_z\ 1]_{nx4}[A_c]_{4x3} \\
&\text{YU:} \quad [0 \quad 1 \quad 0]_{nx3} = [A_x\ A_y\ A_z\ 1]_{nx4}[A_c]_{4x3} \\
&\text{ZD:} \quad [0 \quad 0 \quad 1]_{nx3} = [A_x\ A_y\ A_z\ 1]_{nx4}[A_c]_{4x3} \\
&\text{ZU:} \quad [0 \quad 0 \quad -1]_{nx3} = [A_x\ A_y\ A_z\ 1]_{nx4}[A_c]_{4x3}
\end{aligned} \tag{11}$$

Since the values of the matrices $[A_a]$ and $[A_m]$ are known, the value of the matrix $[A_c]$ can be obtained using the matrix form of the least squares method;

$$[A_c] = ([A_m]^T.[A_m])^{-1}.[A_m]^T.[A_a] \tag{12}$$

2.3 Compass Calibration

Thus, the measurements taken from the accelerometer and magnetic field sensors are calibrated simultaneously and the magnetic direction angle is determined. Before converting to magnetic direction angle, the slope of the sensor to the front, back and sides is calculated using accelerometer values. The slope correction is made by rotating the magnetic field components in the opposite direction of the slope in both directions. In this way, magnetic field values, which are changed due to the slope, are transformed into values parallel to the flat surface, and the direction angle is calculated correctly.

The rotations made around the sensor axes are shown in Figure 3. Let the angle made by the sensor around the X axis is Rx, around the Y axis is Ry, and around the Z axis is Rz. The so-called rotation matrix is used to find the angles Rx, Ry and Rz based on the accelerometer data and calculated as follows (Equation 13).

$$\begin{aligned}
RM_x &= \begin{bmatrix} 1 & 0 & 0 \\ 0 & \cos R_x & \sin R_x \\ 0 & -sinR_x & \cos R_x \end{bmatrix} \\
RM_Y &= \begin{bmatrix} \cos R_Y & 0 & -\sin R_Y \\ 0 & 1 & 0 \\ \sin R_Y & 0 & \cos R_Y \end{bmatrix} \\
RM_z &= \begin{bmatrix} \cos R_Z & \sin R_z & 0 \\ -\sin R_z & \cos R_z & 0 \\ 0 & 0 & 1 \end{bmatrix}
\end{aligned} \tag{13}$$

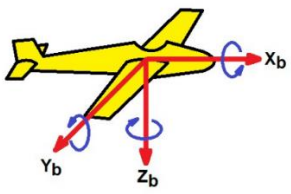

Figure 3. Axial rotational movements of the sensor

Calibrated values of the acceleration sensors give a value of 1 under gravity. When the sensor is parallel to the ground, the acceleration sensor values are X = 0, Y = 0 and Z = 1. These values, when multiplied by rotation matrices, give calibrated values of the acceleration sensors. While RM_x, RM_y and RM_z represents rotation matrices around the X, Y and Z axes respectively, calibrated sensor measurement values;

$$\begin{bmatrix} A_x \\ A_y \\ A_z \end{bmatrix} = [RM_x].\left[RM_y\right].[RM_z]\begin{bmatrix} 0 \\ 0 \\ 1 \end{bmatrix} \tag{14}$$

Using Equation 14, the expressions are found as follows.

$$\left.\begin{aligned} RM_X &= \arcsin\left(\frac{A_Y}{\cos RM_Y}\right) \\ RM_Y &= \arcsin(-A_x) \end{aligned}\right\} \tag{15}$$

After this step, slope correction can be applied on the calibrated values of the magnetic field sensor. M_{XT}, M_{YT} and M_{ZT} are the slope corrected magnetic field measurements of the X, Y and Z axes respectively. The magnetic field measurements are calculated as follows.

$$\begin{bmatrix} M_{XT} \\ M_{YT} \\ M_{ZT} \end{bmatrix} = [M_X]^{-1}.[M_Y]^{-1}.\begin{bmatrix} M_x \\ M_Y \\ M_Z \end{bmatrix} = \begin{bmatrix} \cos R_Y & 0 & \sin R_x \\ \sin R_x \sin R_y & \cos R_x & -\sin R_x \cos R_Y \\ -\cos R_X \sin R_Y & \sin R_x & \cos R_x \cos R_y \end{bmatrix}\begin{bmatrix} M_x \\ M_y \\ M_z \end{bmatrix} \tag{16}$$

As a result of these processes, the slope of the magnetic field sensor values is corrected and made parallel to the ground surface. Only the X and Y components of the magnetic field values are used to find the magnetic direction angle. The Z component is used for tilt correction only. Direction angle is calculated as follows;

$$\beta = \arctan\left(\frac{M_{YT}}{M_{XT}}\right) \tag{17}$$

Since the arctan function values are within ± 90° range, the following correction should be made to calculate the angle value between 0-360°;

- If $M_{XT} > 0$ & $M_{YT} \geq 0$ then $\beta = \arctan\left(\frac{M_{YT}}{M_{XT}}\right)$
- If $M_{XT} < 0$ then $\beta = 180 + \arctan\left(\frac{M_{YT}}{M_{XT}}\right)$
- If $M_{XT} > 0$ & $M_{YT} < 0$ then $\beta = 360 + \arctan\left(\frac{M_{YT}}{M_{XT}}\right)$
- If $M_{XT} = 0$ & $M_{YT} < 0$ then $\beta = 90^o$
- If $M_{XT} = 0$ & $M_{YT} > 0$ then $\beta = 270^o$

3. RESULTS AND DISCUSSION

The error graph of the PSO fitness function is given in Figure 4. Here PSO is trying to bring the error closer to zero. The red line is the filtered version of all samples shown in blue, with a floating average of 100 samples.

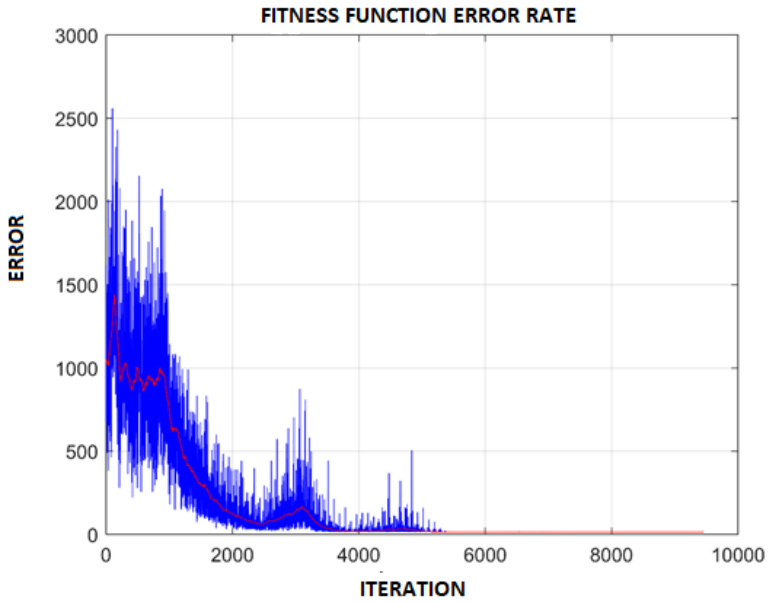

Figure 4. PSO fitness function error graph

The slope error is the slope of the graph of the plane vector and the vertical vector. For example, while the Z axis is facing down, the X axis and Y axis are parallel to the plane. The slope value of the ZX graph is found by fitting the first order polynomial. In this way, slopes are found for all sample sets and the square root of all the square is taken and summed (Figure 5).

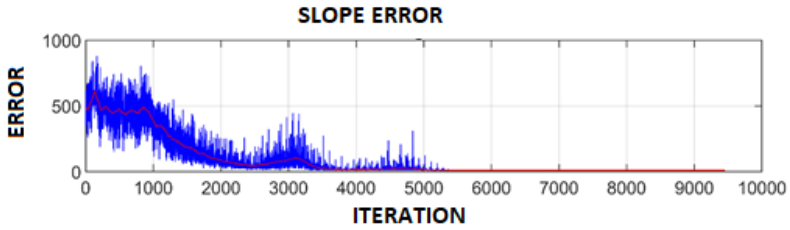

Figure 5. Slope error graph

The circle fitness error checks for the circle resemblance to the shape of planar vector pairs. In doing so, the vector sum of each pair of samples in the sample group is expected to give the same value (circle radius). For this, the magnitude of the vector sum of the plane vector pair is computed for each value of the sample set. Then their variance is taken and divided by the total number of samples (Figure 6).

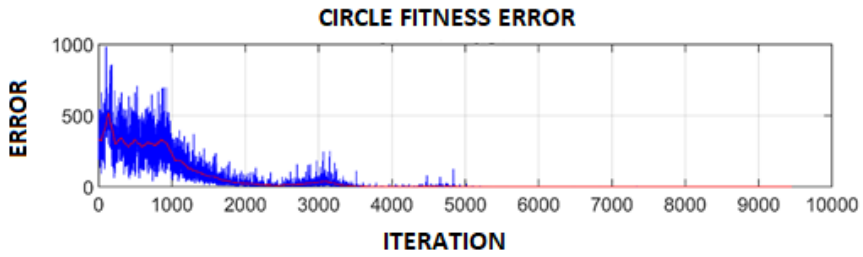

Figure 6. Circle fitness error graph

For the sphere fitness error, all groups in the sample set are combined and the vectoral total for each sample is calculated. The variance of the amplitude of the vector sum of each sample is taken and multiplied by the correction coefficient. In order to obtain a smooth sphere, the variance is tried to be brought closer to zero (Figure 7).

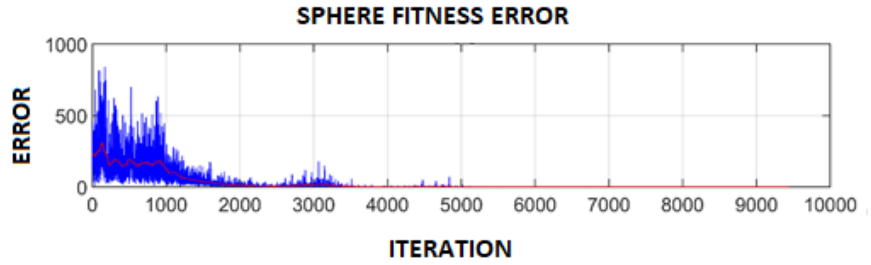

Figure 7. Sphere fitness error graph

Figure 8 shows the sample set corrected with PSO. Red stars that have not yet scaled to the unit circle indicate the reference circle. The sample circle and the reference circle overlap.

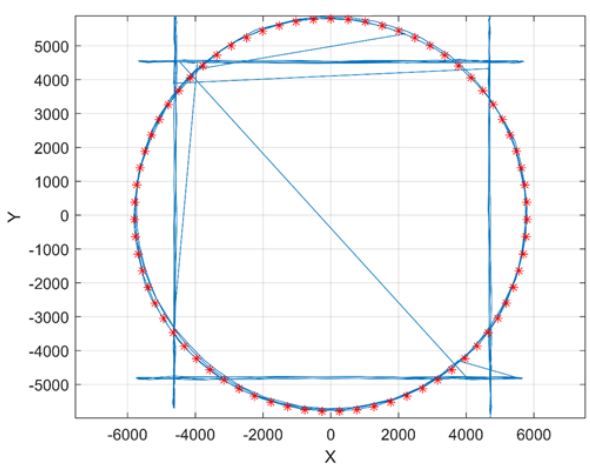

Figure 8. Corrected sample set

Figure 9 shows the normal distribution graph of the amplitude of the vector sum of XYZ axes after calibration. It shows that all samples are located on the unit sphere.

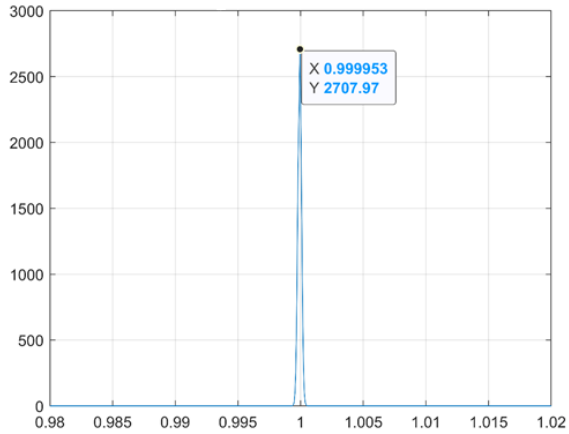

Figure 9. Normal distribution graph

Many errors related to MEMS sensors are mentioned in the literature. For magnetic field sensors, there are errors caused by external factors such as hard metal effect and soft metal effect, as well as scaling error, offset error, inter-sensor interaction error and structural errors. The hard metal effect is caused by metals that change the direction of the natural magnetic field. Soft metal effect is caused by alternating currents in the circuit board where the sensor is located. Scaling error is caused by the nature of the sensor. The offset error is caused by the sensors not displaying 0 for zero magnetic field strength. Interference error between sensors is caused by the sensor axes not being perpendicular to each other. In addition, there are structural errors such as the sensors display different values for magnetic field values with equal amplitude but opposite to each other. There are also structural errors such as offset error caused by not being able to display 0 value, inter-sensor interaction error caused by the sensor axes not being exactly perpendicular to each other, and sensors displaying different values for magnetic field values with equal amplitude but in opposite direction to each other. In high-cost MEMS sensor models, since these errors have been corrected, the calibration process can be performed simply by correcting the offset error (hard metal effect and soft metal effect errors are seen as offset error at the sensor output). In the case of low-cost sensors, manufacturers are providing some statistical information about these errors. Most of the time, the heat stress that the sensor is exposed to during the soldering of the electronic card and the mechanical stresses that occur after soldering disrupt the sensor characteristics and cause it to exceed the values provided by the manufacturer.

The most difficult parameter to determine during the calibration of the magnetic field sensor is the parameters of the matrix that show inter-axial interaction errors. In order for these parameters to be determined correctly, the offset and scaling errors of the sensors must be corrected, that is, the sensor values must be able to accurately show the magnetic field value they detect. However, scaling and offset errors cannot be detected precisely because of the interaction error between axes. As a result of the experiments carried out within the scope of the study, it was observed that first rough elimination of the sensor's offset errors greatly reduced the amount of error in the remaining steps of the calibration process. After a rough determination of the offset values, sensor samples are formed into a spherical form when the inter-sensor interference and the rest of the offset error are heuristically compensated.

Because the magnetic field sensor is affected by external factors, substantial errors may occur in the direction angle. For such cases, there is a need to determine when the sensor measurement value can be trusted and when it cannot. In this study, the vector sum of the axis values of the sensor under the natural magnetic field is determined as the parameter to verify the reliability of the sensor.

4. CONCLUSION

The results obtained with the algorithm developed within the scope of the study have an error of approximately ±2° and meet the value specified by the manufacturer in the sensor document. The biggest challenge encountered during sensor calibration is that the reference measurement values are generated from the values collected from the sensor itself. Inherent errors of the sensor, especially the inter-axial interaction matrix values, can be determined with reference to another highly accurate sensor. Thus, by using the values of both the reference sensor and the sensor to be calibrated, a sensor with higher accuracy can be obtained by simply fixing the sensors on the same plane so that they are facing the same direction and moving together.

Since accelerometer values are used in slope compensation, the noise of the slope angles is high. Especially in applications such as navigation, where the sensor needs to move continuously, the noise becomes more and more affecting the direction angle. This situation caused by the accelerometer can be made suitable for mobile applications by adding a gyro sensor to the system and combining both sensor values in the Kalman filter. In addition, the gyro sensor can be used as a reference sensor during the calibration of the magnetic field sensor. However, in addition to all these, the calibration of the gyro sensor and the way to compensate the constantly changing bias value should be considered, and the additional costs it will bring to the system should also be considered.

5. REFERENCES

Barbert G.W., Arrott A.S., History and magnetics of compass adjusting. IEEE Transactions on Magnetics, 6, 2883-2885, 1988.

Bo L., Hongxia P., A hybrid PSO-DV based intelligent method for fault diagnosis of gear-box. 2009 IEEE International Symposium on Computational Intelligence in Robotics and Automation (CIRA), December 15-18, 2009, Daejeon/Korea.

Caruso M. J., Application of magnetic sensors for low-cost compass systems. IEEE 2000 Position location and navigation symposium, March 13-16, 2000 pp:177-184, San Diego, California, ABD.

Cho S.Y. Park C.G., Tilt Compensation Algorithm for 2-Axis Magnetic Compass. Electronics Letters 39(22), 1589-1590, 2003.

Choudhury T., Consolvo S., Harrison B., Hightower J., LaMarca A., LeGrand L., Rahimi A., Rea, A., Borriello G., Hemingway B., Klasnja P., Koscher K., Landay J.A., Lester J., Wyatt D., Haehnel D., The mobile sensing platform: An embedded activity recognition system, Activity Based Computing. IEEE Pervasive Computing 7(2), 32-41, 2008.

Das P.K., Behera H.S., Panigrahi B.K., A hybridization of an improved particle swarm optimization and gravitational search algorithm for multi-robot path planning. Swarm Evol Comput 28(6), 14-2, 2016.

Fang J., Sun H., Cao J., Zhang X., Tao Y., A Novel Calibration Method of Magnetic Compass Based on Ellipsoid Fitting. IEEE Transcations on Instrumentation and Measurement 60(6), 2053-2061, 2001.

Gietzelt M., Wolf K., Marschollek M., Haux, R., Performance Comparison of Accelerometer Calibration Algorithms Based on 3D-Ellipsoid Fitting Methods. Computer Methods and Programs in Biomedicine 111(1), 62-71, 2013.

Gong D.W., Zhang J.H., Robot path planning in uncertain environment using multi-objective particle swarm optimization. Neurocomputing 103(1), 172-185, 2013.

Kamış Kocabıçak Z., Demir U., Design and Optimization of an Electromechanical Actuator for the Latch of a Foldable Vehicle Seat. Component-Oriented Testing and Simulation 62(7), 1-7, 2020.

Kocaoğlu S., Akdoğan E., Design and Development of an Intelligent Biomechatronic Tumor Prosthesis. Biocybernetics and Biomedical Engineering 39(2), 561-570, 2019.

Kuşçu H., Yılmazlar E. Tez T., Examination on Bipedal Robots Structures and Motion Control, Journal of the Technical University of Gabrovo 57, 69-72, 2018.

Li X., Li Z., A New Calibration Method for Tri-Axial Field Sensors in Strap-down Navigation. Measurement Science and Technology 23, 1-6, 2012.

Li Z., Li X., Wang Y., A Calibration Method for Magnetic Sensors and Accelerometer in Tilt-compensated Digital Compass, 9th International Conference on Electronic Measurement & Instruments (ICEMI'2009), Beijing/China, August 16-19, 2009, pp: 868-871.

Mac T.T., Copot C., Tran D.T., A hierarchical global path planning approach for mobile robots based on multi-objective particle swarm optimization. Applied Soft Computing 59 (1), 68-76, 2017.

Petrucha V., Kaspar P., Calibration of a Triaxial Fluxgate Magnetometer and Accelerometer with an Automated Non-Magnetic Calibration System, IEEE Sensors 2009 Conference, New Zealand, October 25-28, 2009, pp: 1510-1513.

Vcelak J., Ripka P., Platil A., Kubik J., Kaspar P., Errors of AMR Compass and Methods of Their Compensation, Sensors and Actuators A: Physical 129, 53-57, 2006.

Wu Y., Coordinated path planning for an unmanned aerial-aquatic vehicle (UAAV) and autonomous underwater vehicle (AUV) in an underwater target strike mission. Ocean. Engineering 182(6), 162-173, 2019.

Xisheng L., Ruiqing K., Xiongying S., Guanghua Y., Tilt-Induced-Error Compensation for 2-Axis Magnetic Compass with 2-Axis Accelerometer, 2009 World Congress on Computer Science and Information Engineering, Los Angeles, California, USA, March 31-April 2, 2009 pp: 122-125.

Zhang P., Milios E.E., Huynh P., Navigation with IMU / GPS / Digital Compass with Unscented Kalman Filter, 2005 IEEE International Conference on Mechatronics & Automation, Niagara Falls/Canada, July 29-August 1, 2005, pp: 1497-1502.

Zhang Z., Two-Step Calibration Methods for Miniature Inertial and Magnetic Sensor Units, IEEE Transactions on Industrial Electronics 62(6), 3714-3723, 2015.

Zhao Q., Yue Y., Guan Q., A PSO-Based Ball-Plate Calibration for Laser Scanner, International Conference on Measuring Technology and Mechatronics Automation (ICMTMA 2009), Zhangjiajie/Hunan/China, April 11-12, 2009, pp: 479-481.